Dicle University
Journal of Engineering
https://dergipark.org.tr/tr/pub/dumf
duje.dicle.edu.tr

Research Article

# Determination of the Effects of Structural Design Parameters on Dynamic Characteristics of Centrifugal Pump Systems

**Murat ŞEN**[1*]

[1] Fırat University, Engineering Faculty, Mechanical Engineering, msen@firat.edu.tr, Orcid No: 0000-0002-3063-5635

ARTICLE INFO

*Article history*:

Received 17 June 2025
Received in revised form 29 June 2025
Accepted 7 July 2025
Available online 30 September 2025

*Keywords*:

*Campbell Diagram, Centrifugal Pump, Critical Speed, Modal Analysis, Rotordynamic Analysis*

*Doi: 10.24012/dumf.1721157*

* Corresponding author

ABSTRACT

Pump systems are critical in engineering, and their design demands extensive calculations to achieve safety and efficiency. These dynamic systems, with components like shafts, impellers, and bearings, are exposed to various dynamic effects. Therefore, understanding how a pump's dynamic characteristics evolve during the design phase is crucial for ensuring safe, high-performance operation. In this study, modal analysis and rotordynamic analysis were performed on a rotor system, consisting of the shaft, impeller, and bearings of a centrifugal pump system. A numerical model of this system was created using MATLAB. The moving rotor of the centrifugal pump was modeled using the Euler-Bernoulli beam theory. The impeller was represented as an equivalent disk after creating its 3D solid model, taking into account its polar and diametric moments of inertia. The ball bearings supporting the rotor were modeled using linear spring and damping elements. Presented study investigates how the natural frequencies and critical speeds of the rotor system changed for different distances between the two ball bearings used for shaft support and for various bearing stiffness values. Additionally, the presence of anti-resonance frequencies in the transfer frequency response functions between the impeller and the bearings was identified, and their variations with parameter changes were analyzed. The conducted parameter variations revealed that the natural frequencies and critical speeds changed significantly, and these changes exhibited different tendencies depending on the mode shapes. The results demonstrate that constructional design parameters in pump system rotors significantly influence the system's dynamic characteristics.

## Introduction

Rotor systems are designed to operate at certain rotation speeds. Dimensions of rotor systems, material properties, and design of bearing and support systems are made according to many engineering calculations. One of the most important issues to consider in rotor systems is the calculation of natural frequencies and critical rotation speeds of the rotors. Physical and mechanical properties of rotor systems, bearing conditions and operating conditions are the features that affect natural frequencies and critical speeds. The operating speeds of the rotors should be determined to be far from critical speeds. A rotor system has many critical speeds, and when any of these critical speeds is exceeded, operating conditions in this region can be considered safe until it approaches the other critical speed value. However, it is desired that the rotor exceeds critical speeds as quickly as possible and moves away from this danger zone. If possible, critical speeds should be moved as far away from the operating speed region as possible.

It is seen that rotating rotors are used in many mechanical systems in engineering applications. One of these is pump systems that enable water transfer from an area at a lower altitude to an area at a higher altitude. Although there are many types of pumps used for this purpose, all pump systems have rotating rotor elements and impellers. Therefore, it is of great importance to consider natural frequencies and critical speeds during the design phase of pumps and to take the necessary precautions at this stage. The length and diameter of the pump rotor, distances between bearings and the type of bearings used have very important effects on these features. Designers and researchers carry out many studies in this context. Huang et al. [1], have studied the rotor blade modes of the turbomolecular pump. They modeled the rotor blades with a simpler equivalent approach based on the basic invariance principle of mass and moment of inertia, and demonstrated the accuracy of this approach with experimental modal analyzes on a real pump system. Minette et al. [2], used the experimental modal analysis method to determine the natural frequency and damping parameters of an electric submersible pump installed in a test well. They used the single-input, multiple-output (SIMO) technique in their modal analysis studies. The results obtained showed that the submersible pump examined had resonance frequencies in the operational operating frequency region between 30 and 62 Hz. In such cases, resonance frequency zones in the operating range should be crossed as quickly as possible, or structural modifications can be made in the system under appropriate conditions.

In some cases, reduction of resonance frequencies or structural modifications can be desired in design studies of pumps. Mohamed and Azmir [4] carried out design modification studies to reduce the natural frequencies of a water purification pump. For this purpose, they made analyzes by making material modifications in the pump system they modeled numerically and placing flexible bearing elements under the pump body, and examined the effects of these modifications on the resonance frequencies. Ashri et al. [3] carried out numerical modal analysis studies to see the effects of the number of blades and impeller disc thickness of the centrifugal pump impeller on the natural frequency and vibration mode shapes. They determined that the increase in the number of blades of the pump impeller and the increase in the impeller disc thickness had an increasing effect on the natural frequencies. In another study, Wang et al. [17] carried out studies to determine the optimum values of the pump impeller's outlet diameter, outlet width, vane angle, number of windings and number of vanes in order to reduce vibration effects and to increase the performance of centrifugal pumps. Rad [11] examined the effects of disc thickness, blade thickness and blade profiles on the dynamic properties of a radial flow impeller with numerical and experimental modal analysis. In [12], machine learning techniques were used to increase the stability and performance of pump impellers. Efforts have been made to increase resonance safety margins and minimize wing mode deformations. Al-Obaidi and Alhamid [16], conducted numerical and experimental investigations into how transient flow conditions affect pressure pulsation phenomena in axial flow pumps. Their study specifically examined the pressure pulsation characteristics and the impeller flow field under varying flow rates and blade angles. They observed that as the flow rate decreased, pump stability diminished, leading to increased pressure pulsations.

Construction parameters and flow dynamic interactions in pump systems have significant effects on the dynamic characteristics of the system. Egusquiza et al. [15] studied experimentally and numerically the dynamic behavior of the impeller of a large pump-turbine unit. They obtained the natural frequencies and mode shapes of the impeller. In order to see the effect of the rotor and supporting structures on the dynamic behavior of the impeller, they analyzed the impeller separately. D'Addio et al. [6] performed numerical dynamic analyzes of a small-sized centrifugal pump used in automotive applications. They determined that a finite element (FE) model with a flexible shaft, concentrated masses and elastic supports made it possible to determine a more meaningful Campbell diagram and harmonic response in a relatively short time. In another study, Yong et al. [7] analyzed the natural vibration frequencies of the impeller of a horizontal flow pump in water by considering the fluid-rotor structure interaction. They determined that the natural frequencies decreased due to the water environment and the damping distribution of the water mass led to the reduction of the amplitude of the impeller in water.

In pump shaft-impeller systems, various necessary analyses can be conducted through modal tests on the actual system. Based on the obtained analysis results, essential measures can be taken or certain modifications can be implemented on the real system. For instance, Baginski et al. [5] investigated the dynamic behaviors of a vertical motor cooling compressor using experimental modal analysis and forced vibration tests. They observed the critical speeds of the rotor and the vibration amplitudes within the critical operating range. A similar study was performed for a centrifugal pump by Oza and Shah [8].

In addition, numerical methods are also used for rotor dynamics and modal analysis of many pump systems. The dynamic characteristics of pump systems with numerical models can be determined by analyzing them with numerical methods. In addition, the created numerical models can be actively used to meet the requirements such as model updating of pump systems. Briend et al. [10] performed dynamic analysis studies on a model of a vehicle rotor mounted on hydrodynamic bearings using the Timoshenko beam model. White et al. [14] performed linear and nonlinear analyses of a multistage vertical pump. They characterized the bearings in the rotor system by their stiffness and damping coefficients. In [9], stress analysis and modal analysis of a screw centrifugal pump were carried out numerically and the pressure distribution on the impeller blades and changes in natural frequencies were investigated. Guo and Du [13] investigated the dynamic characteristics of the gear pump by performing numerical modal analysis of its components and the entire structure.

In this study, FE model of a centrifugal pump was developed using MATLAB to perform dynamic analyses. The moving rotor of the centrifugal pump was modeled using the Euler-Bernoulli beam theory. The impeller was represented as an equivalent disk after creating its 3D solid model, taking into account its polar and diametric moments of inertia. The ball bearings supporting the rotor were modeled using linear spring and damping elements.

The presented research investigated how changes in distances between bearings and variations in bearing stiffness, defined as design parameters, affected the resonance frequencies and critical speeds of the pump system. Frequency Response Functions (FRFs) were calculated and plotted between selected coordinates of the rotor-impeller system to illustrate resonance peaks. Rotor critical speeds were calculated and presented using Campbell Diagrams. Additionally, the presence of anti-resonances in the transfer FRFs between bearing coordinates and the impeller was examined.

## Methodology

The shaft of the pump system was modelled using the Euler Bernoulli approach. One of the Euler-Bernoulli beam element is given with Figure 1.

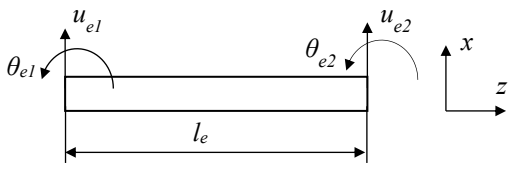


Figure 1. The coordinates of the Euler-Bernoulli beam element on *x-z* plane

In Figure 1, $u_{e1}$ and $u_{e2}$ represent the translational coordinates in *x-z* plane, $\theta_{e1}$ and $\theta_{e2}$ are the rotational coordinates about *y* axis and the coordinates of each element of the shaft can be written as follows:

$$\{q_e\} = \{u_{e1}, \theta_{e1}, u_{e2}, \theta_{e2}\}^T \tag{1}$$

Each node in the shaft element has 2 degrees of freedom (DoF), while each beam element possesses a total of 4 DoFs. The corresponding element-based stiffness and mass matrices are provided below.

Stiffness matrix of the beam element:

$$[k_s]^{(i)} = \begin{bmatrix} k_{11}^{(i)} & k_{12}^{(i)} & k_{13}^{(i)} & k_{14}^{(i)} \\ k_{21}^{(i)} & k_{22}^{(i)} & k_{23}^{(i)} & k_{24}^{(i)} \\ k_{31}^{(i)} & k_{32}^{(i)} & k_{33}^{(i)} & k_{34}^{(i)} \\ k_{41}^{(i)} & k_{42}^{(i)} & k_{43}^{(i)} & k_{44}^{(i)} \end{bmatrix} \tag{2}$$

$$= \frac{E_i I_i}{l_i^3} \begin{bmatrix} 12 & 6l_i & -12 & 6l_i \\ 6l & 4l_i^2 & -6l_i & 2l_i^2 \\ -12 & -6l_i & 12 & -6l_i \\ 6l_i & 2l_i^2 & -6l_i & 4l_i^2 \end{bmatrix} \quad (i = 1, 2, \ldots, n)$$

Where, $E_i$, $I_i$ and $l_i$ are the modulus of elasticity, moment of inertia and the length of the beam elements respectively and $[k_s]_{(i)}$ represents the stiffness matrix.

Mass matrix of the beam element:

$$[m_s]^{(i)} = \begin{bmatrix} m_{11}^{(i)} & m_{12}^{(i)} & m_{13}^{(i)} & m_{14}^{(i)} \\ m_{21}^{(i)} & m_{22}^{(i)} & m_{23}^{(i)} & m_{24}^{(i)} \\ m_{31}^{(i)} & m_{32}^{(i)} & m_{33}^{(i)} & m_{34}^{(i)} \\ m_{41}^{(i)} & m_{42}^{(i)} & m_{43}^{(i)} & m_{44}^{(i)} \end{bmatrix} \tag{3}$$

$$= \frac{\rho_i A_i l_i}{420} \begin{bmatrix} 156 & 22l_i & 54 & -13l_i \\ 22l_i & 4l_i^2 & 13l_i & -3l_i^2 \\ 54 & 13l_i & 156 & -22l_i \\ -13l_i & -3l_i^2 & -22l_i & 4l_i^2 \end{bmatrix} \quad (i = 1, 2, \ldots, n)$$

Where, $\rho_i$, $A_i$ and $[m_s]_{(i)}$ are the mass density, cross-section area and the mass matrix of the beam element. The shaft to be modelled is given in Figure 2.

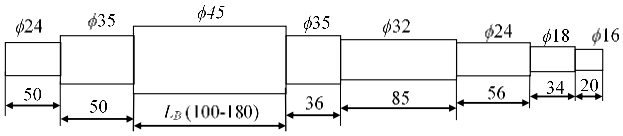


Figure 2. The shaft model of the pump system

In the rotor FE model, the shaft is divided into 8 segments with different diameters and lengths and 9 nodes are created.

For a single disk representing the impeller, its mass matrix can be formulated to account for both its mass and its diametral mass moments of inertia. This matrix captures the contributions from the translational and rotational coordinates at the specific node where the disk is connected within the rotor system.

$$[m_d] = \begin{bmatrix} m_d & 0 \\ 0 & I_d \end{bmatrix} \tag{4}$$

The mass of the disk $m_d$ corresponds to the translational coordinate, while the mass moment of inertia $I_d$ corresponds to the rotational coordinate and these values can be obtained as follows:

The disk's mass ($m_d$) is assigned to the translational coordinate, and its mass moment of inertia ($I_d$) corresponds to the rotational coordinate. These values are determined as follows:

$$m_d = \frac{\rho_d \pi \left(D_d^{\,2} - D_s^{\,2}\right) t_d}{4} \tag{5}$$

$$I_d = \frac{\rho_d \pi \left(D_d^{\,4} - D_s^{\,4}\right) t_d}{64} + \frac{\rho_d \pi \left(D_d^{\,2} - D_s^{\,2}\right) t_d^{\,3}}{48} \tag{6}$$

In Equations 5 and 6, $\rho_d$, $D_d$, $D_s$ and $t_d$ represent the mass density, the outer diameter, the inner diameter and the thickness of the disk, respectively.

After obtaining the matrices of all the elements in the shaft-impeller system, the general stiffness and mass matrices of the system can be created as given with Figure 3.

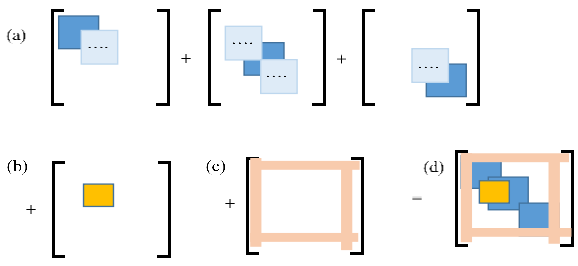


Figure 3. The matrices of the rotor system; (a) shaft, (b) disk (impeller), (c) bearings (constraints), (d) the overall system [18]

In Figure 3 (c), the illustrated section represents the constraints imposed by the bearings. Depending on the bearing type, either translational or rotational coordinates can be restricted to establish pinned or fixed boundary conditions.

However, in this study's rotor model, boundary conditions were not directly applied at the bearing coordinates. Instead, the bearings were modeled using grounded spring and damping elements. This approach, dictated by the construction's requirements, allows for a more realistic solution by incorporating the effects of these bearings into the system in this manner. Furthermore, if desired, pinned or fixed boundary conditions can still be achieved by modeling the bearings with very high spring stiffness values (Figure 4).

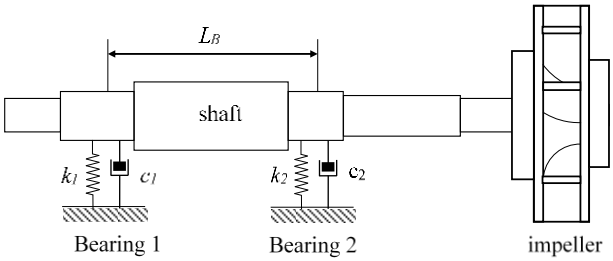


Figure 4. Shaft, impeller, bearing system

After the global mass and the stiffness matrices of the entire system are created, the equation of motion of the system can be written as follows:

$$[M]\{\ddot{q}\}+[C]\{\dot{q}\}+\Omega[G]\{\dot{q}\}+[K]\{q\}=\{f\} \qquad (7)$$

By using Equation 7 and with the eigenvalue solution, the dynamic analysis can be made for the rotor system numerically.

The 3D model of the designed pump system, including all its components, is presented as an assembled view in Figure 5 below.

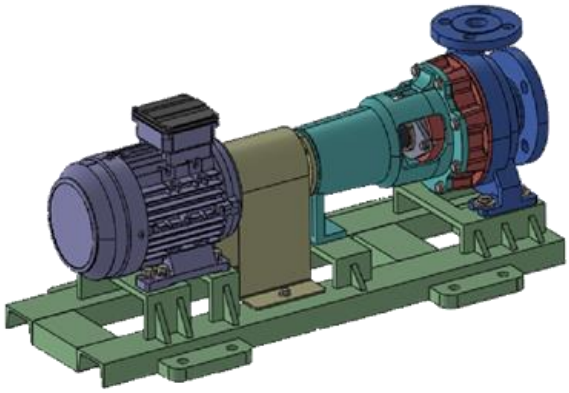

Figure 5. 3D assembly of the pump system

Typically, in such systems, the base chassis supporting the entire system also influences its dynamic characteristics. The rigidity of the areas where the electric motor, pump housing, and bearing unit casing are connected, along with the screwing and assembly techniques, directly affect the system's vibration characteristics. However, the focus of this study is the pump system's rotor group, specifically the subsystem composed of the shaft, impeller, and bearings (Figure 6).

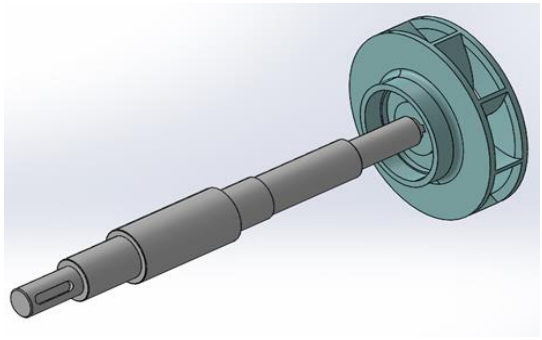

Figure 6. Shaft-impeller system of the centrifuge pump

The mechanical properties of the shaft and the impeller are given in Table 1.

Table 1. Mechanical properties of the system

| Property | Shaft | Impeller |
|---|---|---|
| Modulus of Elasticity (GPa) | 205 | 200 |
| Mass Density (kg/m$^3$) | 7850 | 7800 |
| Polar Mass Moment of Inertia (kg-m$^2$) | 5.74x $10^{-3}$ | 0.49 x $10^{-3}$ |
| Diametral Mass Moment of Inertia (kg-m$^2$) | 3.63x $10^{-3}$ | 27.13 x $10^{-3}$ |

Equation 8 was used to calculate FRFs numerically.

$$\alpha_{pq}(\omega)=\sum_{r=1}^{N}\frac{\phi_{pr}\phi_{qr}}{\left(k_r-\omega^2 m_r\right)+i\eta_r k_r} \qquad (8)$$

Here $\phi_{pr}$ and $\phi_{qr}$ are the elements of the $r^{th}$ mode shape vector at coordinates $p$ and $q$, $k_r$, $m_r$ and $\eta_r$ are the modal stiffness, modal mass and modal damping ratio of the $r^{th}$ mode, respectively. $\omega$ represents the circular frequency in rad/s.

## Simulation Studies

The simulation studies consist of three stages. In the first stage, the natural frequency values and critical speeds of the system were examined for different values of the distance between the bearings for which the bearing springs were modeled with equal and constant (5x10$^6$ N/m).

In the second stage, in the case where the distance between the bearings was constant (140 mm), how changing the stiffness of the identical bearings affected the natural

frequency values and critical speeds of the system were examined.

In the third stage, the anti-resonance frequencies in the transfer FRFs between the coordinate of the impeller and the coordinate of each shaft bearing were determined. In this way, the frequency values of the shaft bearings that will not be affected by the imbalances that may occur in the pump impeller are determined. This feature can be used in the design phase of many rotor systems in order to solve vibration problems.

For the first stage of simulations, the bearing stiffness values were $5x10^6$ N/m and identical for both bearings. For different distance between the bearings, the calculated resonance frequencies for the first 5 bending vibration mode shapes are given in Table 2.

Table 2. Natural frequencies of the shaft, impeller, bearing system for different bearing distances

| $L_B$ (mm) | Natural Frequencies (Hz) | | | | |
|---|---|---|---|---|---|
| | Modes | | | | |
| | 1 | 2 | 3 | 4 | 5 |
| 100 | 15.09 | 187.13 | 498.41 | 895.66 | 1503.40 |
| 120 | 16.97 | 195.88 | 521.96 | 863.65 | 1520.99 |
| 140 | 18.77 | 204.32 | 540.32 | 838.38 | 1536.94 |
| 160 | 20.57 | 212.57 | 548.98 | 825.95 | 1542.52 |
| 180 | 22.44 | 220.69 | 544.74 | 829.52 | 1534.96 |

For the distance 140 mm, one point and one transfer FRF are given with Figure 7.

In Figure 7, the upward peaks represent the natural frequencies and the downward peaks represent the anti-resonance frequencies. Since natural frequencies are a global property of the system, they appear in all FRFs. However, since anti-resonance frequencies are a local property of the system, they may appear in some FRFs but not in others. Due to the property of point FRFs, an anti-resonance frequency appears after each natural frequency in point FRFs.

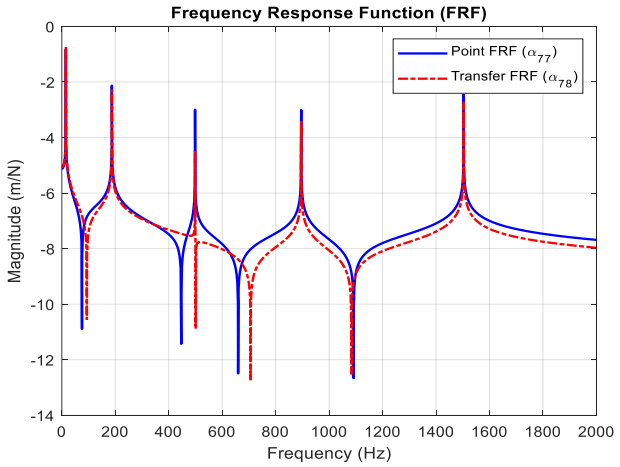


Figure 7. Point and transfer FRF samples of the system for 140 mm distance between the bearings.

For one of the simulations in Table 1, the mode shapes were obtained as given in Figure 8.

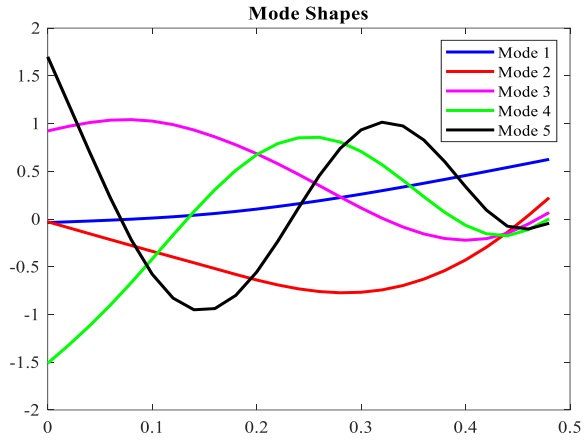


Figure 8. Mode shapes of the shaft, impeller, bearing rotor system of the pump for 140 mm bearing distance

The mode shapes illustrated in Figure 8, can differ for different configurations.

In rotor dynamics analysis, with the rotation of shaft influences the stiffness of the rotor and affects the natural frequencies. This situation can be analyzed using Campbell diagrams which indicate speed dependent damped natural frequencies and the critical speeds. The critical speeds were obtained for all simulations for the first stage of simulations. The obtained critical speed values are given in Table 3 and one of the Campbell diagram for 140 mm bearing distance is given with Figure 9. The operating speed of the designed pump was determined as 2900 rpm. Therefore, when calculating the rotor critical speeds and drawing Campbell diagrams, the speed range of 0-5000 rpm was examined. However, it should be noted that in some special pump systems, speeds can even exceed 10000 rpm. In such cases, a wider speed range should be examined.

Table 3. Critical speeds of the shaft, impeller, bearing system for different bearing distances

| $L_B$ (mm) | Critical Speeds (rpm) | | | | |
|---|---|---|---|---|---|
| | 1 | 2 | 3 | 4 | 5 |
| 100 | 956 | 978 | - | - | - |
| 120 | 1090 | 1118 | - | - | - |
| 140 | 1216 | 1252 | - | - | - |
| 160 | 1340 | 1384 | - | - | - |
| 180 | 1464 | 1520 | - | - | - |

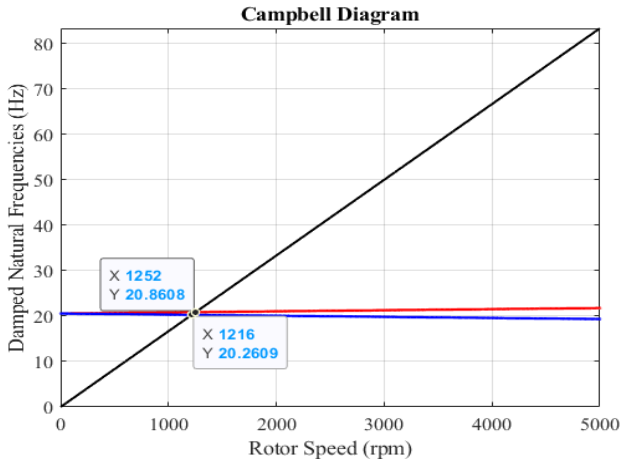


Figure 9. Campbell diagram of the system for 140 mm distance between the bearings.

In the second stage of simulations, for 140 mm distance between the bearings, the natural frequencies of different bearing stiffness values were calculated and the obtained values are given in Table 4.

Table 4. Natural frequencies of the shaft-impeller system for different bearing stiffness

| Bearing Stiffness (N/m) | Natural Frequencies (Hz) Modes | | | | |
|---|---|---|---|---|---|
| | 1 | 2 | 3 | 4 | 5 |
| $2x10^6$ | 15.39 | 184.57 | 414.16 | 667.88 | 1411.96 |
| $4x10^6$ | 18.05 | 199.83 | 508.29 | 789.03 | 1495.84 |
| $6x10^6$ | 19.30 | 207.77 | 567.15 | 881.79 | 1576.71 |
| $8x10^6$ | 20.03 | 212.73 | 610.34 | 955.51 | 1650.84 |
| $10x10^6$ | 20.50 | 216.14 | 643.88 | 1017.44 | 1716.58 |

One point and one transfer FRF are given with Figure 10 for $6x10^6$ N/m bearing stiffness.

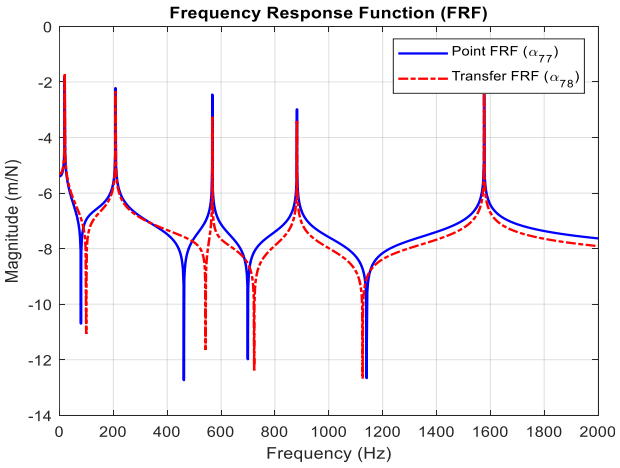


Figure 10. Point and transfer FRF samples of the system for $6x10^6$ N/m bearing stiffness.

The calculated critical speeds are tabulated in Table 5 and one of the Campbell diagrams, for $6x10^6$ N/m bearing stiffness, is illustrated with Figure 11.

Table 5. Critical Speeds of the shaft-impeller system for different bearing stiffness

| Bearing Stiffness (N/m) | Critical Speeds (rpm) | | | | |
|---|---|---|---|---|---|
| | 1 | 2 | 3 | 4 | 5 |
| $2x10^6$ | 950 | 972 | - | - | - |
| $4x10^6$ | 1156 | 1188 | - | - | - |
| $6x10^6$ | 1260 | 1300 | - | - | - |
| $8x10^6$ | 1326 | 1370 | - | - | - |
| $10x10^6$ | 1370 | 1416 | - | - | - |

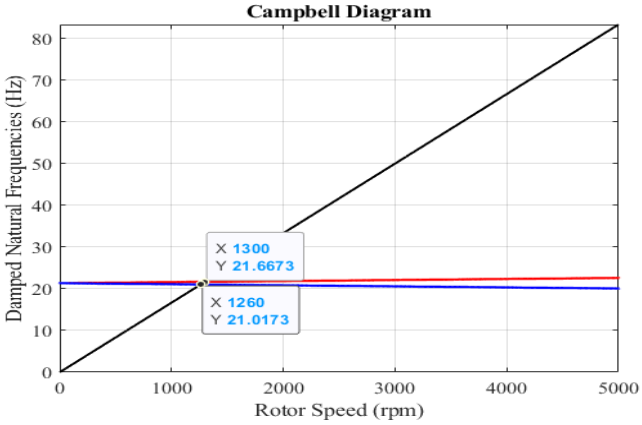


Figure 11. Campbell diagram of the system for $6x10^6$ N/m bearing stiffness.

For the third stage of the simulations, anti-resonance frequencies were investigated.

In a rotor system comprising a shaft, impeller, and bearings, the presence of anti-resonance frequencies can be crucial for enhancing the system's dynamic stability and efficiency. These frequencies provide insights into whether harmonic forces arising from imbalances are transmitted to the bearings. If an anti-resonance frequency exists in the transfer FRF between two coordinates in a mechanical system, one coordinate remains stationary despite the harmonic force excitation occurring at the other. This phenomenon can serve as a solution for many vibration problems. Consequently, in the third stage of this study, the existence of anti-resonance frequencies in the transfer FRFs between the impeller coordinate, which has a high potential for generating harmonic forces due to imbalances, and the bearing coordinates, which are the most vulnerable components in the system, was investigated in detail.

Calculated anti-resonance frequencies are presented in Table 6-9 for the coordinates between the impeller and the bearings. Specifically, these frequencies are provided for Bearing 1 (FRF: $\alpha_{3,9}$) and Bearing 2 (FRF: $\alpha_{4,9}$), considering various distances between the bearings and different bearing stiffnesses, respectively.

Table 6. Anti-resonance frequencies of the shaft-impeller system for different bearing distances for $\alpha_{3,9}$

| $L_B$ (mm) | Anti-resonance Frequencies (Hz) | | | | |
|---|---|---|---|---|---|
| | Modes | | | | |
| | 1 | 2 | 3 | 4 | 5 |
| 100 | - | 358.22 | 862.88 | - | - |
| 120 | - | 347.16 | 859.89 | - | - |
| 140 | - | 328.65 | - | 859.26 | - |
| 160 | - | 307.92 | - | 861.48 | - |
| 180 | - | 288.33 | - | 866.82 | - |

Table 7. Anti-resonance frequencies of the shaft-impeller system for different bearing stiffness $\alpha_{3,9}$

| Bearing Stiffness (N/m) | Anti-resonance Frequencies (Hz) | | | | |
|---|---|---|---|---|---|
| | Modes | | | | |
| | 1 | 2 | 3 | 4 | 5 |
| $2x10^6$ | 271.71 | - | - | 851.65 | - |
| $4x10^6$ | - | 276.76 | - | 856.45 | - |
| $6x10^6$ | - | 380.15 | 862.38 | - | - |
| $8x10^6$ | - | 479.27 | 869.69 | - | - |
| $10x10^6$ | - | 568.98 | 878.90 | - | - |

Table 8. Anti-resonance frequencies of the shaft-impeller system for different bearing distances $\alpha_{4,9}$

| $L_B$ (mm) | Anti-resonance Frequencies (Hz) | | | | |
|---|---|---|---|---|---|
| | Modes | | | | |
| | 1 | 2 | 3 | 4 | 5 |
| 100 | - | - | 860.27 | 1198.68 | - |
| 120 | - | - | 859.82 | 1047.25 | - |
| 140 | - | - | - | 855.62<br>960.10 | - |
| 160 | - | - | - | 834.79<br>917.96 | - |
| 180 | - | - | - | 796.87<br>907.46 | - |

Table 9. Anti-resonance frequencies of the shaft-impeller system for different bearing stiffness $\alpha_{4,9}$

| Bearing Stiffness (N/m) | Anti-resonance Frequencies (Hz) | | | | |
|---|---|---|---|---|---|
| | Modes | | | | |
| | 1 | 2 | 4 | 4 | 5 |
| $2x10^6$ | - | - | 657.48 | 883.96 | - |
| $4x10^6$ | - | - | - | 827.86<br>911.20 | - |
| $6x10^6$ | - | - | 863.81 | 1018.98 | - |
| $8x10^6$ | - | - | 868.84 | 1127.10 | - |
| $10x10^6$ | - | - | 870.71 | 1218.26 | - |

After the anti-resonance frequencies were calculated, as presented in Table 6-9, these computed values were populated into the relevant sections of the tables based on the natural frequencies of the total five bending modes. For instance, an anti-resonance frequency calculated to be between the first and second natural frequencies was placed in the cell corresponding to the first mode. In some cases, more than one anti-resonance frequency was calculated between two natural frequencies, and these were all entered into the cells under the same mode number in the tables.

## Conclusions

In this study, the dynamic properties of the rotor system consisting of shaft, impeller and bearings of a centrifugal pump under different design parameters were investigated. The design parameters in the study were selected entirely in a constructional sense.

This study investigates the influence of the distance between two identical ball bearings and different stiffness values for constant distance, on the natural frequencies and critical speeds of the system. Additionally, anti-resonance frequencies observed in the transfer FRFs between the impeller and each of the two bearings were calculated. The significant outcomes derived from the three-stage simulation studies are as follows:

1. In the initial simulation stage, dynamic analyses were performed on a system utilizing identical bearings, each with a stiffness of $5x10^6$ N/m. The distance between these two bearings was progressively increased by 20 mm increments, from 100 mm to 180 mm (i.e., 100, 120, 140, 160, and 180 mm). The resulting natural frequencies were then compiled.

   It was observed that, generally, increasing the distance between the bearings led to an increase in natural frequency values, with the exception of mode 4. The most significant increase, at 23.75%, was noted in mode 1, while the smallest increase, 2.05%, occurred in mode 5. A different trend was observed for mode 4, where increasing bearing distances resulted in a decrease in natural frequencies, calculated at -7.97%. This inverse relationship could potentially be attributed to the specific positioning of the bearings at those distances and their corresponding zero points.

   Assuming that the pump shaft rotates at 2900 rpm, critical speeds between 0-5000 rpm were calculated and two critical speed values were determined in each simulation. It is seen that the critical speed values increase with the increase in the distance between the bearings. This increase was calculated as 34.69% in the first critical speed and 35.65% in the second critical speed.

2. In the second simulation stage, with the bearing distance held constant at 140 mm, the system's natural frequencies were calculated and listed for varying bearing stiffnesses of (2, 4, 6, 8, and 10)$x10^6$ N/m. A consistent trend was observed across all modes: as bearing stiffness increased, the natural frequency values also tended to rise. The most significant increase, at 35.67%, was found in mode 3, while the smallest increase, 14.57%, occurred in mode 2

   Additionally, two critical speed values were identified in these simulations. As bearing stiffness values increased, the critical speeds also demonstrated an

upward trend. This increase was calculated to be 30.65% for the first critical speed and 31.35% for the second critical speed.

3. In the third simulation stage, anti-resonance frequencies were investigated. The existence of anti-resonances in the transfer FRFs between the impeller and the bearings and how they are influenced by the change of the distance between the bearings and the change of the bearing stiffness values were investigated.

   In the transfer FRF ($\alpha_{3,9}$) between the impeller and the far-side bearing (the one distant from the impeller), no anti-resonance was observed following the natural frequency of the first mode. However, for the second mode, an anti-resonance was consistently present after the natural frequency across all investigated bearing distances. Furthermore, the frequency values of these anti-resonances increased as the distance between the bearings expanded. After the natural frequencies of the other modes, anti-resonances were observed in some simulations but not in others.

   As bearing stiffness values increased, a corresponding increase in the values of the observed anti-resonance frequencies was noted. It was also observed that while anti-resonances appeared after the resonance frequencies in some modes during certain simulations, they were not identified in others. The absence of an anti-resonance after the natural frequency in Mode 5 is considered normal, as the frequency response curve typically terminates in this region.

4. In the transfer FRF ($\alpha_{4,9}$) between the impeller and the central bearing (the one closer to the impeller), no anti-resonance was found following the natural frequencies of the first and second modes. However, after the natural frequency of mode 4, two anti-resonances were consistently observed across different bearing distances. Notably, as the distance between the bearings increased, the frequency values of these anti-resonances decreased. For the natural frequencies of other modes, anti-resonances were present in some simulations but absent in others.

   With an increase in bearing stiffness values, the anti-resonance frequencies observed also showed an increase. Similar to the previous findings, anti-resonances were sometimes visible after the resonance frequencies in certain modes during simulations, but not always identified in others.

In conclusion, this study demonstrates that bearing distance and bearing stiffness values can be effectively utilized as design parameters to enhance the efficiency and performance of pump systems. These parameters were found to directly and significantly influence the system's dynamic behavior. Furthermore, it was emphasized that anti-resonance frequencies are similarly affected by these parameters and can also be leveraged during the design phase of pump systems.

## Ethics committee approval and conflict of interest statement

There is no conflict of interest with any person / institution in the article prepared.

## Authors' Contributions

The author confirms sole responsibility for the following: Study conception and design, acquisition of data, analysis and interpretation of data, drafting of manuscript, critical revision.

## References

[1] Z. Huang, B. Han, and Y. Le, "Modeling method of the modal analysis for turbomolecular pump rotor blades", Vacuum, vol. 144, pp. 145-151, 2017.

[2] R.S. Minette, S.F. SilvaNeto, L.A. Vaz, and U.A. Monteiro, "Experimental modal analysis of electrical submersible pumps", Ocean Engineering, vol. 124, pp. 168–179, 2016.

[3] M. Ashri, S. Karuppanan, S. Patil, and I. Ibrahim, "Modal Analysis of a Centrifugal Pump Impeller Using Finite Element Method", MATEC Web of Conferences, 13, 0403 0 (2014).

[4] M.F.B. Fasal Mohamed, and N.A.B. Azmir, "Study on behavior of water treatment pump before and after modification using finite element modal analysis", IOP Conf. Series: Materials Science and Engineering824 (2020) 012004.

[5] P. Bagiński, A. Andrearczyk, P. Ziółkowski, "Investigation of the dynamic behaviour of the vertical rotor of a refrigeration compressor supported by foil bearings", Renewable Energy 253 (2025) 123505.

[6] V. D'Addio, P. Forte, F. Frendo, and R. Squarcini, "Rotordynamic analysis of a centrifugal pump for automotive applications", Procedia Structural Integrity 24 (2019) 510–525.

[7] S. Yong, W. Donglei, J. Tao1, and L. Yanwei, "Modal Analysis on Impeller Rotor of the Axial Flow Pump based on Fluid-structure Interaction", IOP Conf. Series: Earth and Environmental Science 376 (2019) 012023.

[8] M.N. Oza, D.S. Shah, "Theoretical and experimental modal analysis of centrifugal pump radial flow impeller", IOP Conf. Series: Materials Science and Engineering 992 (2020) 012003 IOP Publishing, doi:10.1088/1757-899X/992/1/012003.

[9] S.Q. Yuan, T. Li, J.P. Yuan, and J.J. Zhou, "Static stress and modal analysis on the impeller of screw centrifugal pump", IOP Conf. Series: Earth and

Environmental Science, 15 (2012), 052013doi:10.1088/1755-1315/15/5/052013.

[10] Y. Briend, M. Dakel, E. Chatelet, M. Andrianoely, R. Dufour, and S. Baudin, "Effect of multi-frequency parametric excitations on the dynamics of on-board rotor-bearing systems" Mechanism and Machine Theory 145 (2020) 103660.

[11] S.Z. Rad, "Finite element, modal testing and modal analysis of a radial flow impeller", Iranian Journal of Science & Technology, Transaction B, Engineering, Vol. 29, No. B2.

[12] L. Xin, Q. Li, and Y. Liu, "Dynamic analysis of the impeller under optimized blade design for a pump-turbine", Journal of Energy Storage 107 (2025) 114900.

[13] F. Guo and H. Du, "Modal Analysis of Components and Whole of Gear Pump", IOP Conf. Series: Earth and Environmental Science 632 (2021) 032005, doi:10.1088/1755-1315/632/3/032005.

[14] M.F. White, E. Torbergsen, and V.A. Lumpkin, "Rotordynamic analysis of a vertical pump with tilting-pad journal bearings", Wear 207 (1997) 128–136.

[15] E. Egusquiza, C. Valero, A. Presas, X. Huang, A. Guardo, and U. Seidel, "Analysis of the dynamic response of pump-turbine impellers. Influence of the rotor", Mechanical Systems and Signal Processing, 68-69, (2016), 330–341.

[16] A.R. Al-Obaidi and J. Alhamid, "Analyses of the transient turbulence flow in a 3D impeller axial pump using Novel vibration signals and Inner dynamic simulation techniques", Flow Measurement and Instrumentation 102 (2025) 102779.

[17] K. Wang, G. Luo, Y. Li, R. Xia, and H. Liu, "Multi-condition optimization and experimental verification of impeller for a marine centrifugal pump", International Journal of Naval Architecture and Ocean Engineering 12 (2020) 71e84.

[18] Şen M., Çakar O., and Yiğid O., "Model reduction and dynamic analysis of a rotor system", VI-International European Conference on Interdisciplinary Scientific Research, August 26-27, 2022 / Bucharest, Romania, pp: 317-329.